ORIGINAL PAPER

Strong acid-assisted preparation of green-emissive carbon dots for fluorometric imaging of pH variation in living cells

Qin Wang[1] · Haitao Yang[1] · Qiang Zhang[1] · Hongguang Ge[1] · Shengrui Zhang[1] · Zhiyin Wang[1] · Xiaohui Ji[1]

Abstract

New green-emissive carbon dots (G-CDs) are described here and shown to be viable fluorescent nanoprobes for the detection of changes in cellular pH values. By using *m*-phenylenediamine as the carbon source, G-CDs with an absolute quantum yield of 36% were solvothermally synthesized in the presence of strong H_2SO_4. The G-CDs have an average size of 2.3 nm and display strong fluorescence with excitation/emission peaks at 450/510 nm. The fluorescence intensity depends on the pH value in the range from 6.0 to 10.0, affording the capability for sensitive detection of intracellular pH variation. The nanosensor with excellent photostability exhibited good fluorescence reversibility in different pH solutions, and showed excellent stability against the influence of other biological species. The nanoprobe was successfully used in confocal fluorescence microscopy to determine pH values in SMMC-7721 cells.

Keywords Carbon nanoparticles · Nanoprobes · *m*-Phenylenediamine · Assistance of H_2SO_4 · Fluorescence · Quantum yield · Excellent photostability · Intracellular pH change · Bioimaging · Real-time sensing

Introduction

Intracellular pH plays an important role in many physiological and pathological cellular events such as cell apoptosis and endocytosis [1], calcium regulation [2], and tumor growth [3]. Deviation in pH value in cellar organelles (even 0.10–0.20 pH units in either direction from a pH of 7.40) is linked to several human diseases, such as cancer, cardiopulmonary and neurological problems [4, 5]. As pH distribution and variation in living cells are related to many cellular functions, sensitive and selective probes for monitoring pH values in living cells are crucial for better understanding the biological effects of pH gradients.

Fluorescent pH indicators have attracted much more attention than other methods, due to their high sensitivity and selectivity, excellent spatial/temporal resolution, real-time and in situ imaging [6]. To date, through the measurement of changes in fluorescence intensity, three strategies have been explored to conveniently and reliably detect pH values in living cells. One method employs organic dyes as fluorophores to construct small-molecule-based pH sensors [7, 8]. However, such pH indicators may suffer from relatively tedious procedures, and rapid photo bleaching, which make long-term imaging difficult. Alternatively, fluorescent proteins are also widely used as fluorophores for the determination of pH value in living cells [9, 10]. However, a potential drawback of this strategy is the complicated extraction and purification steps. In addition to these strategies, nanomaterial-based fluorescence pH sensors have been employed for monitoring pH value in living cells.

Recently, carbon dots (CDs) have been applied for pH detection due to their high photostability, excellent solubility, and favorable biocompatibility [11–14]. However, most of such reported nanoprobes suffer from the general problem of short wavelength emission, which may be subjected to several disadvantages, such as severe photo-damage to living organisms, and the auto-fluorescence of the biological matrix [15, 16]. To overcome these limitations, substantial effort has been made to enhance the fluorescence quantum yield (QY) and shift the wavelength of nanosensor to the longer-wavelength region [17, 18]. However, the exploration of CD-based

✉ Xiaohui Ji
slgjxh@163.com

1   Shaanxi Key Laboratory of Catalysis, School of Chemistry and Environment Science, Shaanxi University of Technology, Hanzhong 723000, Shaanxi, China

fluorescence nanoprobes with long-wavelength emission and high QY for monitoring pH variation in living cells still remains at an early stage.

Toward this end, we synthesized bright-green-emissive CDs (G-CDs) with a high QY of 36% as fluorescence pH sensors and then applied them for intracellular pH sensing. The G-CDs demonstrating remarkable fluorescence emission at 510 nm were synthesized through the one-pot solvothermal treatment of m-phenylenediamine (m-PD). The G-CDs, exhibiting a pK_a value of 7.95, displayed a good linear relationship with pH variation in the range of 6.0–10.0 in buffer (Scheme 1). Moreover, the nanosensor exhibited good photostability and reversibility and showed excellent sensitivity and specificity toward pH over other biological analytes and microenvironment factors. Thus, due to their remarkable physicochemical properties, the G-CDs can be applicable for real-time monitoring of pH changes in living cells.

Experimental section

Chemicals and materials

m-Phenylenediamine m-PD), cysteine (Cys), glutathione (GSH), homocysteine (Hcy), HClO, H_2O_2, metal ions and other amino acids were all purchased from Aladdin Ltd. (http://www.aladdin-e.com/, Shanghai, China). All other reagents were of analytical grade and used as received without further purification. Distilled water was used throughout this study.

Instruments

Transmission electron microscopy (TEM) images were taken on a GZF2.0 FEI Electron Optics (Thermo Scientific, America https://www.thermofisher.com/). X-ray powder diffraction (XRD) analysis was performed using an X-ray diffractometer (Bruker, Germany https://www.bruker.com/) with Cu-Kα radiation ($\lambda = 1.5178$ Å). X-ray photoelectron spectroscopy (XPS) was performed on an ESCALAB 250Xi

multitechnique surface analyzer (Thermo Scientific, America https://www.thermofisher.com/). Fourier transform infrared (FT-IR) spectra were collected on a Tensor 27 FT-IR spectrometer (Bruker, Germany https://www.bruker.com/), using KBr pellets. Absorption measurements were recorded using a Shimadzu UV-2550 spectrophotometer (Shimadzu, Japan https://www.shimadzu.com). All fluorescence spectra were measured on a RF5301 fluorescence spectrometer (Shimadzu, Japan https://www.shimadzu.com). The absolute QY was determined using integrating spheres (150 mm, PTFE inner surface) fitted within an Edinburgh Analytical FLS920 instrument (Techcomp, China http://www.techcomp.cn/). The pH measurements were carried out by using a Sartorius PB-10 pH meter (Sartorius, Germany https://www.sartorius.com.cn/). Mixtures were centrifuged by a Xiangyi H1650-W centrifuge (Xiangyi, China http://www.xiangyihn.com/). Fluorescence imaging was performed by using an Olympus FV1000 confocal laser scanning microscope (Olympus, Japan http://www.olympus.com.cn/).

Preparation of CDs

G-CDs were synthesized by carbonization of m-PD with the assistance of concentrated H_2SO_4 through a solvothermal method. First, m-PD (0.1 g) was dissolved in C_2H_5OH (10 mL). Then, 60 μL of concentrated H_2SO_4 (98%) was added dropwise under vigorous stirring, and the solution was subsequently transferred into a 25 mL poly(tetrafluoroethylene)-lined stainless steel autoclave. After being heated at 180 °C for 2 h and cooling to room temperature, a dark-green suspension was obtained. The solution was centrifuged at 12,000 rpm (the centrifugation force was 10,000×g) for 15 min to remove the non-fluorescent precipitates. The products were actually mixtures of CD samples with different emission behaviors (Fig. S1), which were purified via silica column chromatography using a mixture of methylene dichloride and methanol as the eluent (CH_2Cl_2/CH_3OH, 10: 1 v/v), and the G-CDs were selected to construct the nanosensor. After evaporating the solvent and further drying under vacuum, the CD sample was finally obtained.

Scheme 1 Schematic illustration of strong acid-assisted preparation of G-CDs and their application for pH sensing
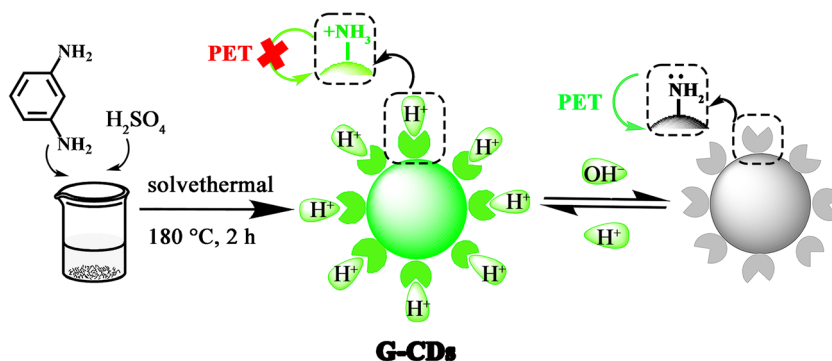
Fluorometric determination of pH value

The G-CDs were dissolved in ethanol to obtain a stock solution. The determination of pH values was performed in 20 mM buffer: phosphoric acid-disodium hydrogen phosphate buffer at pH 2.0, disodium hydrogen phosphate-citric acid buffer at pH 2.2–8.0, glycine-sodium hydroxide buffer at pH 8.5–10.6, and disodium hydrogen phosphate-sodium hydroxide buffer at pH 10.9–12.0. In a set of test tubes, 100 μL of CD dispersion (1.0 mg·mL^{-1}) was added to 4.90 mL buffer at different pH values. The resulting solution was well-mixed, and then the fluorescence spectra were recorded. The measurements were conducted in triplicate.

Cytotoxicity assay

The cytotoxicity of G-CDs was investigated by a standard 3-(4, 5-dimethyl-2- thiazolyl)-2, 5-diphenyl-2H-tetrazolium bromide (MTT) assay. SMMC-7721 cells were seeded in 96-well plates for 24 h before treatment, then cultured with different concentrations of G-CDs (0–60 μg·mL^{-1}) for 12 h. Then, 20 μL of MTT solution (5.0 mg·mL^{-1}) was added to each well, followed by incubation at 37 °C for 4 h. After that, 100 μL of the supernatant was removed, and 150 μL of dimethyl sulfoxide (DMSO) was added to each well to dissolve the formed formazan. The plate was shaken for 10 min, and the absorbance of the solution in the well at 562 nm was measured with a WD-2102A microplate reader (Beijing Liuyi, China http://www.ly.com.cn/). All MTT assays were performed four times in duplicate.

Cell fluorescence imaging

Before experiments, SMMC-7721 cells were plated on 6-well culture plates containing sterile coverslips and allowed to adhere for 24 h. The medium was removed and the cells were treated with G-CDs (40 μg·mL^{-1}) in RPMI medium for 5 h at 37 °C. Subsequently, the cells were rinsed with phosphate buffered saline (PBS) (pH 7.4) three times. It was then treated with 5 μg·mL^{-1} nigericin in high concentration K$^+$ buffer at different pH values (6.0, 6.5, 7.4, 8.0 and 8.5) and incubated further for 30 min. Cell imaging was immediately performed on an Olympus FV1000 confocal laser scanning microscope. Excitation wavelength for G-CDs: 458 nm; emission collection: 475–575 nm. For further intracellular pH imaging, SMMC-7721 cells were first treated with chloroquine (CQ; 200 μM) for 1 h and dexamethasone (DEX; 1 μM) for 6 h. After that, the medium was removed and the cells were rinsed three times. Before imaging, the cells were further incubated with G-CDs (40 μg·mL^{-1}) for 5 h at 37 °C, and cell imaging was performed using the conditions described above.

Results and discussion

Synthesis of CDs

m-PD was chosen as the reactant and concentrated H$_2$SO$_4$ was selected as a carbonization agent because of its strong dehydrating and oxidizing properties. It is worth noting that the volume of concentrated H$_2$SO$_4$ was the key parameter in the formation of the bright G-CDs. As shown in Fig. S2, with increasing volumes of concentrated H$_2$SO$_4$, G-CDs were finally obtained in approximately 0, 2.4, 5.7, 11.4 and 10.9 wt% yields. Thus, the value of 60 μL was found to be optimal. Similarly, a series of optimization experiments of reaction time were performed, and G-CDs were finally obtained in approximately 6.1, 11.9 and 11.3 wt% yields. The optimal time was determined to be 2 h (Fig. S3). Thus, the concentrated H$_2$SO$_4$ not only prompts the generation of G-CDs, but also accelerates the reaction rate of polymerization and carbonization reactions under high temperature and high pressure. Finally, the crude product was critically separated via silica column chromatography to afford G-CDs as a black solid.

Characterization of the green-emissive carbon dots (G-CDs)

First, the morphology of G-CDs was determined by using TEM. As illustrated in Fig. 1, the G-CDs were spherical in shape and showed excellent dispersibility in aqueous solution. Moreover, their size distribution (calculated based on the
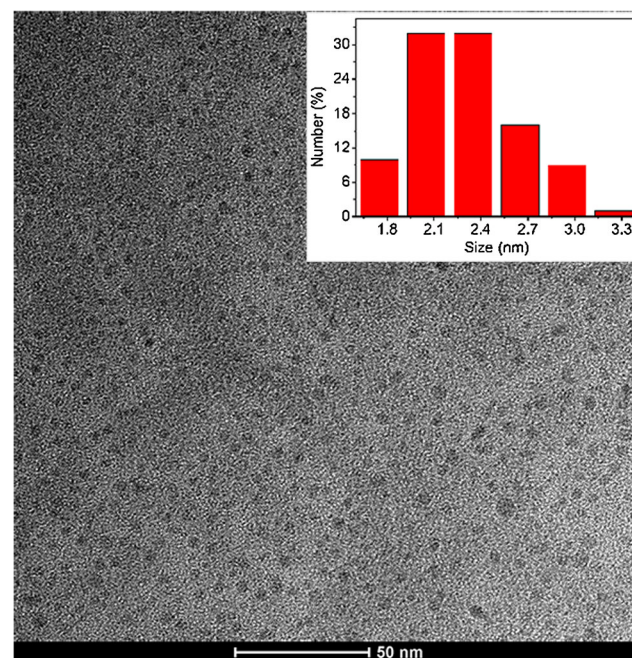

Fig. 1 Size and morphology of G-CDs characterized by TEM image. Inset: histograms of the particle size distribution

measurement of more than 100 particles in the TEM image) was estimated at 1.8–3.3 nm, with an average size of 2.3 nm. XRD was then used to measure the CDs. As shown in Fig. S4, the G-CDs showed a broader peak centered at approximately 25°, which confirms the graphene structure of G-CDs [19].

Subsequently, the elemental compositions and surface functional groups were identified by XPS, and FT-IR spectroscopy, respectively. The survey spectrum indicated that carbon, oxygen, nitrogen, and sulfur are the main components of the desired CDs: 56.13% carbon, 27.16% oxygen, 7.56% nitrogen and 9.15% sulfur (Fig. 2a). In the high-resolution spectra (Fig. 2b–e), the high-resolution C 1 s spectrum can be deconvoluted into three peaks at 285.08, 287.13, and 288.93 eV, corresponding to $C-C/C=C$, $C-N/C-O$, and $O-C=O$ bonds, respectively [20, 21]. The high-resolution N 1 s spectrum shows two peaks at 398.33, and 400.63 eV, representing pyridinic N and

graphitic-like/amino N bonds, respectively [22–24]. The high-resolution O 1 s spectrum peak at 531.83 was attributed to oxygenated carbon atoms ($C=O/C-OH$) [20, 25]. In addition, the S 2p spectrum shows the sulfur signal of $-S(=O)_2-$ at 164.01 eV [26], which may derive from H_2SO_4 added to the reaction mixture, suggesting that H_2SO_4 could react with m-PD through electrophilic reaction and further affect the structure of G-CDs via oxidation, protonation, polymerization, and carbonization reactions. FT-IR characterization was also used to explore the chemical bonds on the surface of G-CDs. Figure 2f depicts the FT-IR spectrum of the G-CDs which shows that the G-CDs possess $-NH_2$ (3388 cm^{-1}), aliphatic CH_2 (2929 cm^{-1}), $O=C-O-$ (1732 cm^{-1}), $C=C$ (1629 cm^{-1}) $-C=N$ (1532 cm^{-1}), $C-N-C$ (1347 cm^{-1}), and $-SO_3H$ (1025 cm^{-1}) functional groups or chemical bonds. The FT-IR and XPS analyses are consistent and provide convincing evidence that $-NH_2$, $-$

Fig. 2 Structure characterization of G-CDs. a XPS survey spectrum; high-resolution XPS survey scans of the (b) C 1 s, (c) N 1 s, (d) O 1 s, and (e) S 2p spectra of G-CDs; and (f) FT-IR spectrum. Each band was deconvoluted following the literature [20–26]
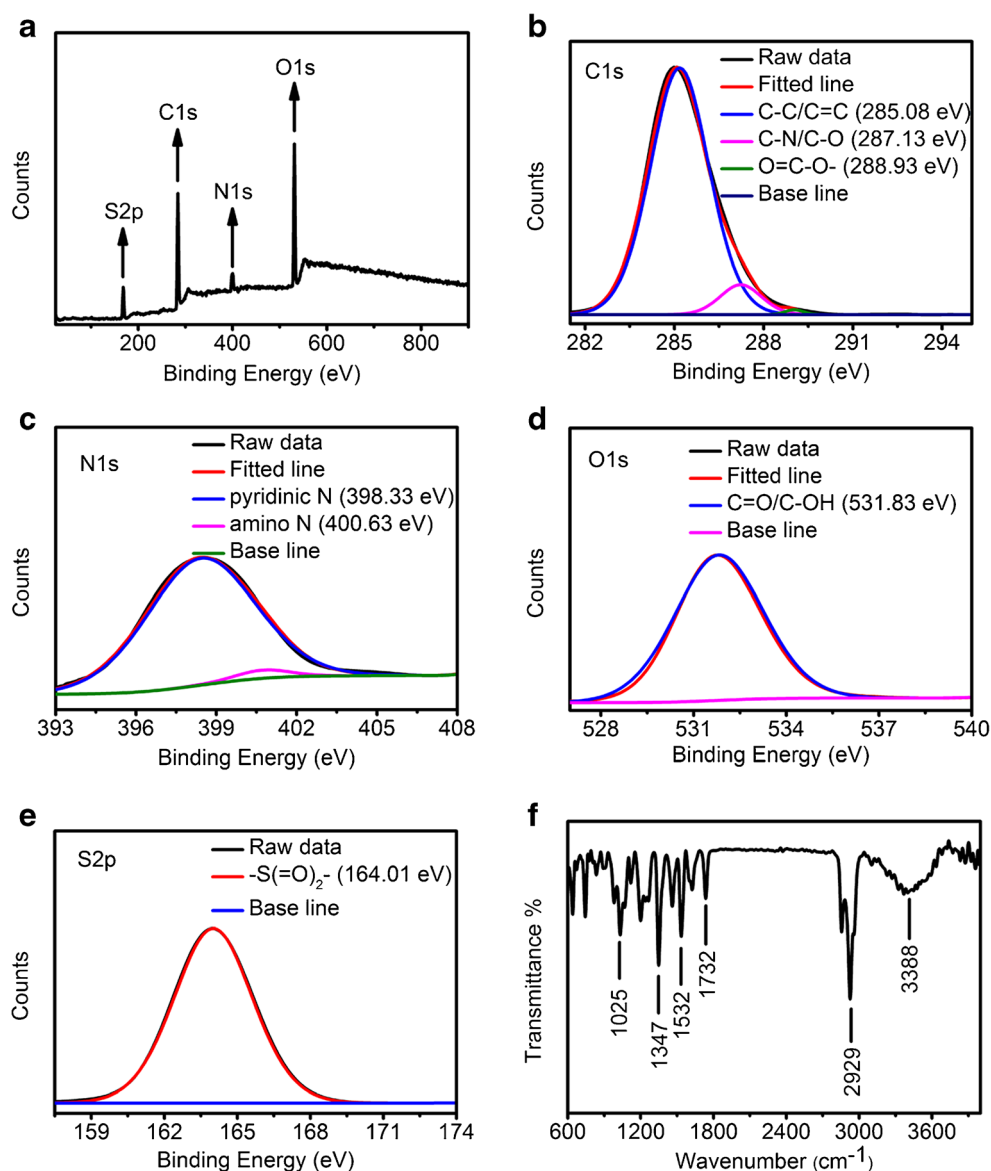
Fig. 3 **a** Fluorescence spectra of G-CDs (20 μg·mL^{-1}) at various pH values (3.0–12.0); Insets in (**a**): photographs of aqueous solutions of G-CDs at pH 6.0 (left) and 10.0 (right); **b** pH-dependent fluorescence intensity changes in G-CDs. $\lambda_{ex}/\lambda_{em} = 450/510$ nm. The corresponding calibration curve for pH (**b**) was measured based on 3 independent measurements
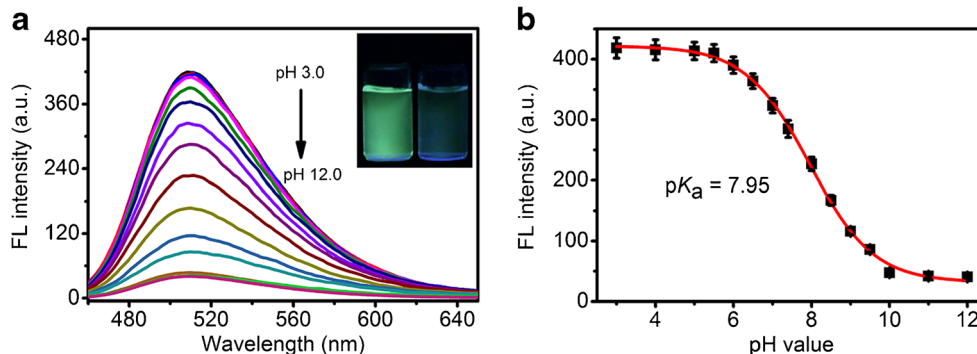

Optical properties of the G-CDs

The absorption and fluorescence spectra of G-CDs were collected to explore their optical properties. Fig. S5 shows that the G-CDs in aqueous solution have several absorption bands at 261 and 340–500 nm. The broad absorption within the range of 340 to 500 nm was assigned to the n − π* transition from the surface states of G-CDs [20]. On the other hand, the single peak observed at 261 nm represents the π–π* transition of aromatic C=C bonds [27]. Next, a detailed investigation of the fluorescence properties of G-CDs was carried out (Fig. S6). The maximum emission wavelength (excited at 450 nm) was 510 nm, and the emission wavelength of G-CDs showed nearly no shift with changes in excitation wavelength ranging from 370 to

490 nm with an interval of 10 nm. This phenomenon indicated that the fluorescence spectra of G-CDs are λ_{ex}-independent and the emission properties of G-CDs mainly depend on the surface states rather than the morphology [28]. The absolute QY of G-CDs was measured to be 36%, which is very high and can effectively overcome the autofluorescence of cells.

Investigation of pH-response properties

Standard fluorescence pH titrations of the G-CDs were performed in 20 mM buffer with different pH values ranging from 3.0 to 12.0. As illustrated in Fig. 3a, with increasing pH values, the fluorescence emission intensity at 510 nm decreased continuously, accompanying an obvious color change observed under UV light (365 nm, insert). Figure 3b shows that sigmoidal fitting of pH dependent fluorescence at 510 nm yields a pK_a value of 7.95. In particular, it was confirmed that the fluorescence intensity at 510 nm is linear with pH variation in the range of 6.0–10.0, according to the linear regression

Fig. 4 Fluorescence intensity of G-CDs (20 μg·mL^{-1}) in 20 mM buffer at different pH values in the presence of 1 mM metal ions: (1) Blank, (2) Na$^+$, (3) K$^+$, (4) Ca^{2+}, (5) Mg^{2+}, (6) Cu^{2+}, (7) Ni^{2+}, (8) Mn^{2+}, (9) Pb^{2+}, (10) Hg^{2+}, and (11) Fe^{3+}; amino acids: (12) Ala, (13) Ser, (14) Thr, and (15) Arg; biothiols: 1 mM GSH (16), 100 μM Cys (17) and 100 μM Hcy (18); and 500 μM ROS: (18) H$_2$O$_2$ and, (19) HClO. **a** pH 5.0, **b** pH 6.0, **c** pH 7.0, and **d** pH 8.0. $\lambda_{ex}/\lambda_{em} = 450/510$ nm. Data are expressed as the mean ± SD of three experiments
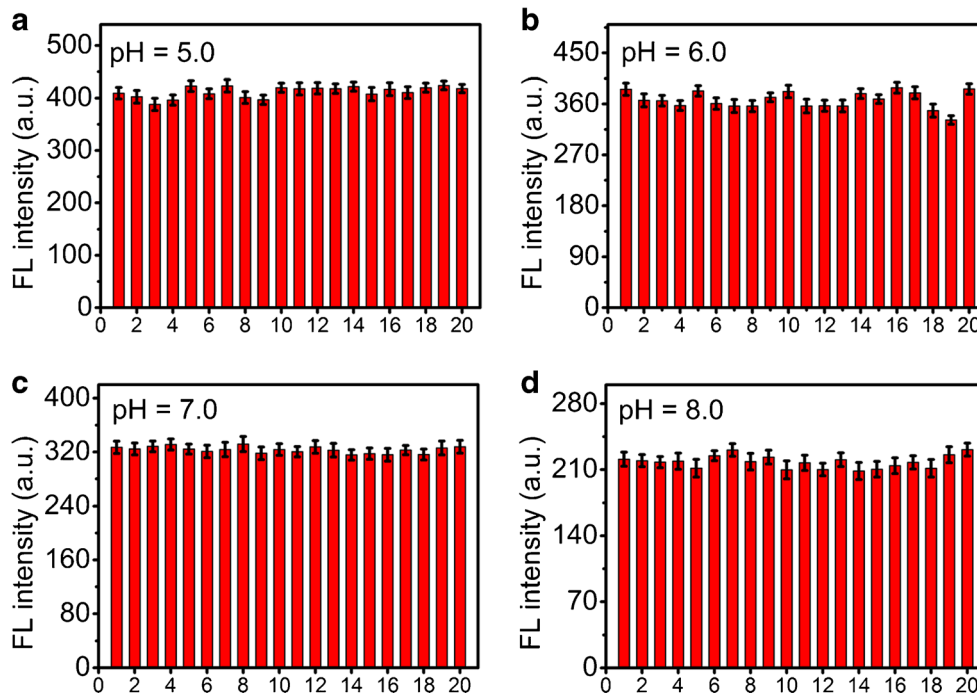
equation $F_{510nm} = -91.04\text{pH} + 9.5 \times 10^2$, with a linear coefficient of 0.9928 (Fig. S7). The linear range is wide and meets the requirement for in vivo imaging and sensing of intracellular pH value. The above results demonstrate that the G-CDs could be applied as a new kind of nanoprobe for the quantitative determination of pH values.

To explore the mechanism for the response to pH value, we investigated the variation in the UV–vis spectra of G-CDs with pH values increasing from 6.0 to 10.0. As shown in Fig. S8, no obvious change could be observed. Therefore, we inferred that the fluorescence quenching of the G-CDs at high pH values might not be attributed to aggregation. Moreover, TEM images of G-CDs at different pH values were collected (Fig. S9). As expected, the average sizes of G-CDs at pH 6.0 and 9.0 were 2.6 and 2.4, respectively, indicating that no aggregation of G-CDs can be observed with increased pH value. On the other hand, it is well known that the photoinduced electron transfer (PET) from aniline to the G-CDs may be feasible at high pH values owing to the aniline lone pair, causing the quenching of fluorescent intensity [29]. Thus, based on the above observation, we supposed that the plausible mechanism for the quenching of the fluorescence of G-CDs with increased pH value could be ascribed to the PET process from the electron lone pair in amino group to the G-CDs (Scheme 1). At high pH value, the excited electrons of G-CDs can jump from the highest occupied molecular orbital (HOMO) to the lowest unoccupied molecular orbital (LUMO), and then, the ground state electron of amino group can transfer to the HOMO of G-CDs due to the fact that the HOMO energy level of amino group is higher than that of G-CDs [29, 30], resulting in obvious fluorescence quenching. In contrast, the lone pair of amino group has been shown to be unavailable for charge transfer when protonation happens [30], and the excited electrons in the LUMO of G-CDs go directly back to the HOMO of G-CDs, restoring the fluorescence intensity.

Photostability and reversibility of G-CDs

The photostability of this nanoprobe was tested by measuring the fluorescent response in 20 mM buffer with different pH values (6.0, 8.0 and 10.0) in daylight and in UV light for 12 h. As shown in Fig. S10, a negligible change in fluorescent emission intensity could be observed during the scanning process at room temperature, indicating that this nanoprobe is superior to organic probes in terms of stability upon long-term daylight and UV light irradiation. Then, the reversible response with respect to pH was tested by repeatedly switching the pH value between 6.0 and 10.0, using NaOH and HCl solution to adjust pH. As shown in Fig. S11, the results clearly revealed that the pH-response fluorescence intensity exhibited well reproducibility between pH 6.0 and 10.0. That is, the nanosensor exhibited good photostability and fluorescence reversibility in different pH value solutions and can be successfully used to monitor intracellular pH variation.
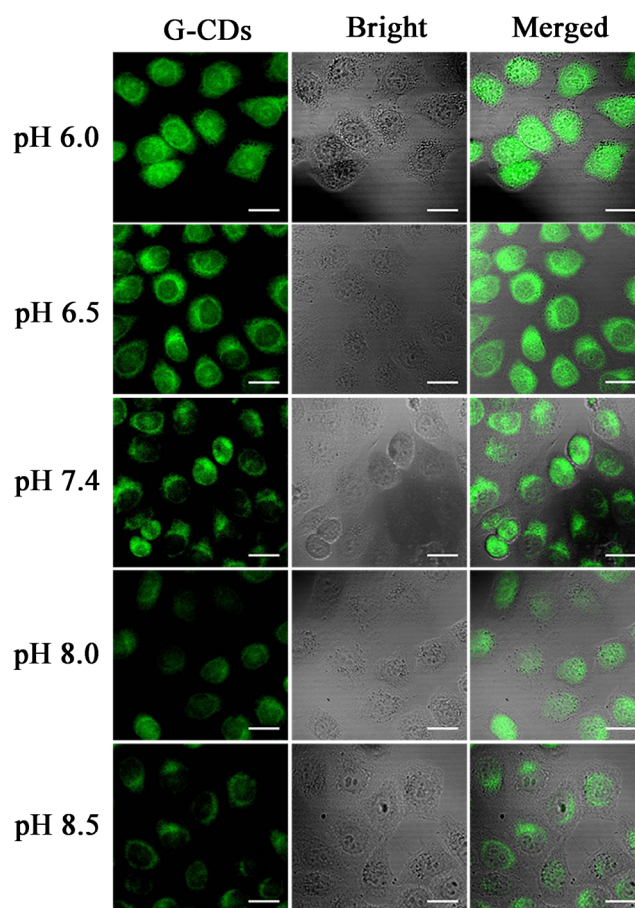
Fig. 5 Confocal fluorescence images of 40 μg·mL^{-1} G-CDs incubated with SMMC-7721 cells in high concentration K$^+$ buffer at different pH values. Excitation wavelength for G-CDs: 458 nm; emission collection: 475–575 nm. Scale bar: 20 μm
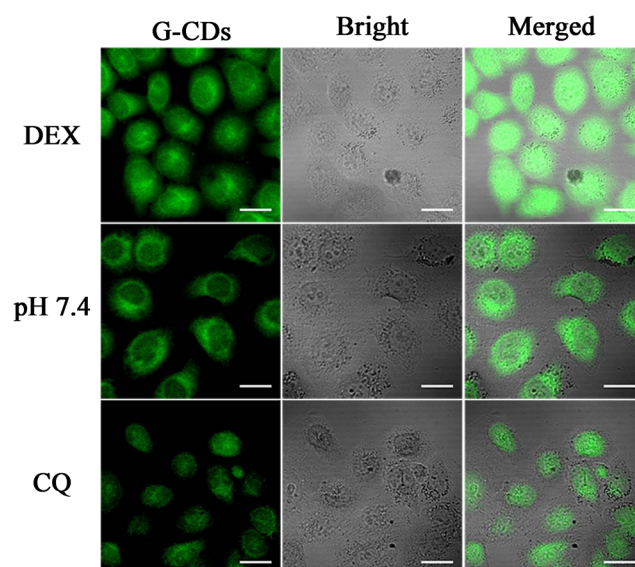
Fig. 6 Confocal microscope analysis of SMMC-7721 cells treated with CQ and DEX. Excitation wavelength for G-CDs: 458 nm; emission collection: 475–575 nm. Scale bar: 20 μm

Table 1 A comparison of nanomaterial-based methods for detection of pH value

Materials	Method	Measurement range (pH values)	Merits	Limitations	Ref.
Carbon nanoparticles	Fluorescence imaging	3.0–12.0	Broad-range pH response	Short wavelength emission	[29]
Synthetic dyes immobilized inside silica nanoparticles	Ratiometric fluorescence imaging	3.0–9.0	Simultaneously measuring pH value and temperature	Relatively complex synthesis procedures	[32]
Carbon dots: EuTbDPA nanoparticles	Absorption / Fluorescence imaging	3.0–10.0	Red light emission	Not real-time monitoring intracellular pH value	[33]
Tricarbocyanine anchored to SiO_2 nanoparticles	Fluorescence imaging	6.0–8.0	Remarkable stokes shift; Near-infrared fluorescent emission	Narrow pH working range	[34]
Polyethylenimine-coated upconversion nanoprobes	Ratiometric fluorescence imaging	4.0–8.0	Ratiometric sensing; Low phototoxicity	Not conducive to cell imaging because of the large particle size	[35]
Carbon dots	Fluorescence imaging	6.0–10.0	Photochemical inertness; Real-time sensing	Short wavelength excitation, but can be improved with the change of surface states	This work

Effect of potential interfering substances in different pH value solutions

For pH sensing in a complex intracellular environment, the potential interference of high concentrations of metal ions (Na^+, K^+, Ca^{2+}, Mg^{2+}, Cu^{2+}, Ni^{2+}, Mn^{2+}, Pb^{2+}, Hg^{2+}, and Fe^{3+}), amino acids (Ala, Ser, Thr, and Arg), biothiols (GSH, Cys and Hcy) and reactive oxygen species (H_2O_2, HClO) was investigated at pH 5.0, 6.0, 7.0 and 8.0. As shown in Fig. 4, no marked changes in fluorescence intensity were observed for G-CDs with respect to these interfering substances, demonstrating the excellent selectivity of this nanoprobe.

To further evaluate the selectivity of the system for the assay of pH value, we investigated the effects of ionic strength and viscosity. As shown in Fig. S12A, a series of pH titrations in buffers with different ionic strengths were performed (0.01, 0.05, 0.10, 0.15, and 0.20 M KCl). No obvious changes were found in the fluorescence emission intensity and peak wavelength, suggesting a negligible effect of ionic strength on the recognition ability of G-CDs. Additionally, we evaluated the effect of viscosity on the emission behavior of G-CDs in methanol/glycerol mixtures with different fractions of glycerol (f_g) (Fig. S12B). The emission intensity of G-CDs still showed no significant changes as the solvent viscosity increased from 0.60 (methanol) to 950 cP (99% glycerol) at room temperature (25 °C) [31]. All these results indicated that this nanoprobe is selective for pH and promising for the detection of pH values in living systems.

pH imaging in living cells

Encouraged by the above-mentioned outcome, the application of G-CDs for imaging pH values in SMMC-7721 cells was carried out. Initially, a standard MTT assay was performed to evaluate the toxicity of G-CDs to living cells. As shown in Fig. S13, no

significant drop in cell viability was observed, indicating that G-CDs pose minimal cytotoxicity to SMMC-7721 cells below 60 μg·mL^{-1}. Subsequently, to measure delicate changes in intracellular pH value, SMMC-7721 cells were first incubated with G-CDs (40 μg·mL^{-1}) for 5 h at 37 °C. Then, the cells were treated with buffer at pH 6.0, 6.5, 7.4, 8.0, and 8.5 for 30 min, which enables the exchange of H^+/K^+ and ensures an equal pH value inside the cells and in the buffer medium. As shown in Fig. 5, the brightest fluorescence images were clearly observed after incubating SMMC-7721 cells in buffer at pH 6.0. With increased pH values ranging from 6.0 to 8.5, the emission intensity of the treated cells decreased gradually. In addition, the average fluorescence intensity was determined (Fig. S14). As expected, the fluorescence intensity was linearly dependent on pH values in the range of 6.0–8.5, which confirmed that the CD-based nanoprobe can quantify delicate changes in intracellular pH value.

To further demonstrate the capability of detecting pH variation in living cells, the pH changes in SMMC-7721 cells induced by CQ and DEX were measured [14]. Compared with the fluorescence intensity of control cells, a remarkable decrease in the brightness of fluorescence cell images was observed in the presence of CQ, and the fluorescence intensities of DEX-treated cells were increased (Fig. 6). Taken together, these results indicated that G-CDs were cell permeable and capable for real-time sensing pH variation in living cells.

Finally, we compared the features of fluorescent methods for pH sensing. As shown in Table 1, previous nanosensors suffer from several disadvantages, such as relatively complex synthesis procedures, blue light emission, or large particle size, making them unsuitable for intracellular studies [29, 32–35]. In contrast, our nanosensor, with an average size of 2.3 nm, shows longer-wavelength emission, chemical and photochemical inertness, which is conducive to bioimaging. The surface functional groups on the nanosensor can be further functionalized for

cellular active-targeting and tracking purposes. The major limitation of the nanosensor is the short excitation wavelength, which can be improved with the change of surface states through incorporating heteroatoms, such as oxygen species [20].

Conclusion

A CD-based fluorescent probe for highly selective measurement of pH variation in SMMC-7721 cells was presented. Using *m*-PD as the carbon source, G-CDs exhibiting an absolute QY of 36% were constructed with the assistance of H_2SO_4 through the green solvothermal treatment of *m*-PD. The G-CDs can be applied to indicate pH values from 6.0 to 10.0 by measuring fluorescence intensity. Owing to their excellent fluorescence photostability, good reversibility and high selectivity toward pH, the nanosensor has been successfully applied to the precise measurement of pH values in SMMC-7721 cells. The mentioned method is a form of nondestructive inspection, which provides maximum protection for the pH measurement of living biological systems. Thus, it is expected that these CD-based nanoprobes can be employed as new promising candidates for intracellular pH sensing in biological systems.

References

1. Kennedy RT, Huang L, Aspinwall CA (1996) Extracellular pH is required for rapid release of insulin from Zn−insulin precipitates in β-cell secretory vesicles during exocytosis. J Am Chem Soc 118: 1795–1796
2. Janecki AJ, Montrose MH, Zimniak P, Zweibaum A, Tse CM, Khurana S, Donowitz M (1998) Subcellular redistribution is involved in acute regulation of the brush border Na^+/H^+ exchanger isoform 3 in human colon adenocarcinoma cell line caco-2: protein kinase C-mediated inhibition of the exchanger. J Biol Chem 273: 8790–8798
3. Zhang X, Lin Y, Gillies RJ (2010) Tumor pH and its measurement. J Nucl Med 51:1167–1170
4. Schindler M, Grabski S, Hoff E, Simon SM (1996) Defective pH regulation of acidic compartments in human breast cancer cells (MCF-7) is normalized in adriamycin-resistant cells (MCF-7adr). Biochemistry 35:2811–2817
5. Izumi H, Torigoe T, Ishiguchi H, Uramoto H, Yoshida Y, Tanabe M, Ise T, Murakami T, Yoshida T, Nomoto M, Kohno K (2003) Cellular pH regulators: potentially promising molecular targets for cancer chemotherapy. Cancer Treat Rev 29:541–549
6. Hou JT, Ren WX, Li K, Seo J, Sharma A, Yu XQ, Kim JS (2017) Fluorescent bioimaging of pH: from design to applications. Chem Soc Rev 46:2076–2090
7. Horak E, Kassal P, Hranjec M, Steinberg IM (2018) Benzimidazole functionalised Schiff bases: novel pH sensitive fluorescence turn-on chromoionophores for ion-selective optodes. Sensor Actuat B: Chem 258:415–423
8. Bao L, Ding L, Hui J, Ju H (2016) A light-up imaging protocol for neutral pH-enhanced fluorescence detection of lysosomal neuraminidase activity in living cells. Chem Commun 52:12897–12900
9. Tantama M, Hung YP, Yellen G (2011) Imaging intracellular pH in live cells with a genetically encoded red fluorescent protein sensor. J Am Chem Soc 133:10034–10037
10. Esposito A, Gralle M, Dani MAC, Lange D, Wouters FS (2008) pHlameleons: a family of FRET-based protein sensors for quantitative pH imaging. Biochemistry 47:13115–13126
11. Mutuyimana FP, Liu J, Na M, Nsanzamahoro S, Rao Z, Chen HL, Chen XG (2018) Synthesis of orange-red emissive carbon dots for fluorometric enzymatic determination of glucose. Microchim Acta 185:518
12. Mutuyimana FP, Liu J, Nsanzamahoro S, Na M, Chen HL, Chen XG (2019) Yellow-emissive carbon dots as a fluorescent probe for chromium (VI). Microchim Acta 186:163
13. Sun YQ, Wang XJ, Wang C, Tong DY, Wu Q, Jiang KL, Jiang YN, Wang CX, Yang MH (2018) Red emitting and highly stable carbon dots with dual response to pH values and ferric ions. Microchim Acta 185:83
14. Shangguan JF, He DG, He XX, Wang KM, Xu FZ, Liu JQ, Tang JL, Yang X, Huang J (2016) Label-free carbon-dots-based ratiometric fluorescence pH nanoprobes for intracellular pH sensing. Anal Chem 88:7837–7843
15. Wang RX, Wang XF, Sun YM (2017) One-step synthesis of self-doped carbon dots with highly photoluminescence as multifunctional biosensors for detection of iron ions and pH. Sensor Actuat B: Chem 241:73–79
16. Hou P, Yang T, Liu H, Li YF, Huang CZ (2017) An active structure preservation method for developing functional graphitic carbon dots as an effective antibacterial agent and a sensitive pH and Al^{3+} nanosensor. Nanoscale 9:17334–17341
17. Park SY, Lee HU, Park ES, Lee SC, Lee JW, Jeong SW, Kim CH, Lee YC, Huh YS, Lee J (2014) Photoluminescent green carbon nanodots from food-waste-derived sources: large-scale synthesis, properties, and biomedical applications. ACS Appl Mater Interfaces 6:3365–3370
18. Liu DY, Qu F, Zhao XN, You JM (2015) Generalized one-pot strategy enabling different surface functionalizations of carbon nanodots to produce dual emissions in alcohol–water binary systems. J Phys Chem C 119:17979–17987
19. Dong YQ, Pang HC, Yang HB, Guo CX, Shao JW, Chi YW, Li CM, Yu T (2013) Carbon-based dots co-doped with nitrogen and sulfur for high quantum yield and excitation-independent emission. Angew Chem Int Edit 52:7800–7804
20. Ding H, Yu SB, Wei JS, Xiong HM (2016) Full-color light-emitting carbon dots with a surface-state-controlled luminescence mechanism. ACS Nano 10:484–491
21. Wang N, Zheng AQ, Liu X, Chen JJ, Yang T, Chen ML, Wang JH (2018) Deep eutectic solvent assisted preparation of nitrogen/chloride doped carbon dots for intracellular biological sensing and live cell imaging. ACS Appl Mater Interfaces 10:7901–7909
22. Wang Y, Lu LL, Peng H, Xu J, Wang FY, Qi RJ, Xu ZA, Zhang W (2016) Multi-doped carbon dots with ratiometric pH sensing properties for monitoring enzyme catalytic reactions. Chem Commun 52:9247–9250
23. Sun S, Zhang L, Jiang K, Wu A, Lin HW (2016) Towards high-efficient red emissive carbon dots: facile preparation, unique

properties, and applications as multifunctional theranostic agents. Chem Mater 28:8659–8668

24. Zhou J, Zhou H, Tang JB, Deng S, Yan F, Li WJ, Qu MH (2017) Carbon dots doped with heteroatoms for fluorescent bioimaging: a review. Microchim Acta 184:343–368

25. Jiang K, Sun S, Zhang L, Lu Y, Wu AG, Cai CZ, Lin HW (2015) Red, green, and blue luminescence by carbon dots: full-color emission tuning and multicolor cellular imaging. Angew Chem Int Edit 54:5360–5363

26. Lindberg BJ, Hamrin K, Johansson G, Gelius U, Fahlman A, Nordling C, Siegbahn K (1970) Molecular spectroscopy by means of ESCA II. Sulfur compounds. Correlation of electron binding energy with structure. Phys Scr 1:286

27. Ge JC, Jia QY, Liu WM, Guo L, Liu QY, Lan MH, Zhang HY, Meng XM, Wang PF (2015) Red-emissive carbon dots for fluorescent, photoacoustic, and thermal theranostics in living mice. Adv Mater 27:4169–4177

28. Wang Q, Zhang SR, Zhong YG, Yang XF, Li Z, Li H (2017) Preparation of yellow-green-emissive carbon dots and their application in constructing a fluorescent turn-on nanoprobe for imaging of selenol in living cells. Anal Chem 89:1734–1741

29. Shi BF, Su YB, Zhang LL, Liu RJ, Huang MJ, Zhao SL (2016) Nitrogen-rich functional groups carbon nanoparticles based fluorescent pH sensor with broad-range responding for environmental and live cells applications. Biosens Bioelectron 82:233–239

30. Hutt JT, Aron ZD (2014) Synthesis and application of ratiometric and "turn-on" fluorescent pH sensors: an advanced organic undergraduate laboratory. J Chem Educ 91:1990–1994

31. Wang YY, Yang XF, Zhong YG, Gong XY, Li Z, Li H (2016) Development of a red fluorescent light-up probe for highly selective and sensitive detection of vicinal dithiol-containing proteins in living cells. Chem Sci 7:518–524

32. Zhang W, El-Reash YGA, Ding LJ, Lin ZZ, Lian Y, Song B, Yuan JL, Wang XD (2018) A lysosome-targeting nanosensor for simultaneous fluorometric imaging of intracellular pH values and temperature. Microchim Acta 185:533

33. Wang L, Chen Y (2018) Lanthanide doped carbon dots as a fluorescence chromaticity- based pH probe. Microchim Acta 185:489

34. Terrones YT, Leskow FC, Bordoni AV, Acebedo SL, Spagnuolo CC, Wolosiuk A (2017) A silica supported tricarbocyanine based pH nanosensor with a large stokes shift and a near infrared fluorescence response: performance in vitro and in live cells. J Mater Chem B 5:4031–4034

35. Näreoja T, Deguchi T, Christ S, Peltomaa R, Prabhakar N, Fazeli E, Perälä N, Rosenholm JM, Arppe R, Soukka T (2017) Ratiometric sensing and imaging of intracellular pH using polyethyleneimine-coated photon upconversion nanoprobes. Anal Chem 89:1501–1508